Electron-electron correlation of $^1S^e$ states of the helium atom

Bao Cheng-guang
Center of Theoretical Physics, Chinese Center of Advanced Science and Technology (World Laboratory), Beijing, China; Department of Physics, Zhongshan University, Guangzhou, China; and Institute of Theoretical Physics, Beijing, China
(Received 26 October 1987)

A nonadiabatic variational procedure is proposed to diagonalize the Hamiltonian of the helium atom. An analysis of the wave functions of the $^1S^e$ states is made. The one-body densities and the shape densities (extracted from two-body densities) are investigated to obtain information on the radial-radial and radial-angular electron-electron correlations. The geometric structure of these states is studied and the K-classification scheme is recovered. Regions where strong radial-angular correlation takes place are found.

I. INTRODUCTION

Since the heliumlike atom is the simplest atom with electron-electron (*e-e*) correlation, a thorough understanding of this system is indispensable in the understanding of the atomic world. There is a long history of investigation of these atoms. Many methods have been proposed, many approximate solutions have been obtained, and the systematics of spectral behavior has been revealed (refer to Refs. 1–3, and references therein). However, there is still a long way to go to understand completely the structure and the internal motion of all the states of these systems.

The focus of the present paper is not on the quantitative aspect. Its aim is to make a detailed and systematic analysis of the wave functions to extract information on *e-e* correlations, to obtain qualitative features of the structure and internal motion of the electrons. For this purpose the following steps are performed.

(i) A procedure is proposed to solve the Schrödinger equation. Only the three lowest series of the $^1S^e$ states of the helium atom are calculated and reported in this paper.

(ii) An evaluation of the accuracy of these solutions is made (it took most of the CPU time of computation).

(iii) The one-body densities are extracted from the wave functions and a systematic analysis of them is made.

(iv) Since in a quantum-mechanical description, the geometric structure of a system is related to its most probable shape, and since the internal motion is just an evolution of shape, it is necessary to define the "shape density" ρ_s, which is the probability density of a given shape at a given orientation.[4] This is an important physical quantity where the details of the *e-e* correlation are stored. We extract the ρ_s from the wave functions, and an analysis of them is made.

(v) Finally, *e-e* correlations and the systematics of the spectrum are discussed.

II. PROCEDURE

The nonrelativistic Schrödinger equation of the helium atom is solved by diagonalizing the Hamiltonian. In this way, two points are worth noting.

(i) The accuracy of the approximate solutions relies seriously on the selection of the basis functions. Thus they must be skillfully selected; otherwise, the convergence will be poor.

(ii) There will be spurious components from the continuum spectrum of the Hamiltonian intruding into the model space spanned by the basis functions. Thus there will be spurious eigensolutions and they must be discriminated from physical solutions.

In selecting the basis functions, it is noticed that there are two possibilities for the geometric configuration of two electrons; either their distances away from the center (the nucleus) are similar or one electron is much farther away than the other. To describe the first possibility, we have chosen three sets of basis functions as

$$\phi^I_{[K]}=(1\pm P_{12})[\psi^{ZI}_{n_1 l_1}(\mathbf{r}_1)\psi^{ZI}_{n_2 l_2}(\mathbf{r}_2)]_L, \quad I=1,2,3 \qquad (1)$$

where $\mathbf{r}_i$ is the position vector of the ith electron, P_{12} stands for an interchange of two electrons, and ψ^{ZI}_{nl} is a modified bound Coulomb wave function (a generalized version of Hylleraas-Shull-Löwdin function[5]). In the usual Coulomb wave function, the argument is Zr/na_0. Evidently, the larger n is, the more remote the electron distribution is. On the other hand, the argument in ψ^{ZI}_{nl} is changed to Zr/Ia_0, where Z is an adjustable parameter of around 2. With this new argument, the distribution of the electron in all different n,l states is restrained in the Ith major shell, resulting in great improvement of the convergence.

For describing the second possibility, we further choose a fourth set composed of the usual bound Coulomb wave functions as

$$\phi^{(4)}_{[K]}=(1\pm P_{12})[\psi^{Z_1}_{n_1 l_1}(\mathbf{r}_1)\psi^{Z_2}_{n_2 l_2}(\mathbf{r}_2)]_L ,$$
$$n_1=1,2,3, \quad n_2>n_1 \qquad (2)$$

where $Z_1=2$ for the inner electron and Z_2 is given as 1.1 for the outer electron.

The basis functions from these four sets (each is truncated) together compose our model space. In the following calculation of the $^1S^e$ states, the model space is 190-

dimensional. This space is not large enough to insure excellent accuracy for all states reported. However, it does give correct qualitative results which we are interested in. Since we do not use an orthonormalized set of basis functions, some of them would be nearly linearly dependent on the others. They have been dropped via an additional orthonormalization procedure.

After the diagonalization of the Hamiltonian, the next job is to find out the spurious solutions. For this purpose, for each eigensolution Ψ_i, we have calculated

$$\eta_i=\frac{\langle\Psi_i\mid H^2-E_i^2\mid\Psi_i\rangle}{E_i^2\langle\Psi_i\mid\Psi_i\rangle}\ . \tag{3}$$

This quantity is a measure of the accuracy. Obviously, the η_i of the spurious eigensolution would be exceptionally large. In the following calculation, it turns out that there are only a few states among the negative eigensolutions having exceptionally large η_i. Thus they can be easily discriminated.

After throwing away the spurious solutions, we can extract from Ψ_i interesting physical quantities. Firstly, we extract the one-body density as

$$\rho_1^i(\mathbf{r}_1)=\int d\mathbf{r}_2\mid\Psi_i\mid^2\ , \tag{4}$$

and

$$\bar{\rho}_1^i(\mathbf{r}_1)=4\pi r_1^2\rho_1^i(\mathbf{r}_1)\ . \tag{5}$$

Secondly, we define and extract the shape density as follows: Instead of using $\mathbf{r}_1$ and $\mathbf{r}_2$, we use a new set of variables where the degrees of freedom associated with the collective rotation decouple with those associated with internal oscillations. Those are the three Euler angles (denoted by $\mathcal{R}$) together with

$$\xi=(r_1^2+r_2^2)^{1/2}\ , \tag{6}$$

describing the size, and with

$$\alpha=\tan^{-1}(r_2/r_1)\ , \tag{7}$$

and θ_{12}, the angle between $\mathbf{r}_1$ and $\mathbf{r}_2$, describing the deformation. The quantities ξ, α, and θ_{12} together determine the shape and are simply denoted by $\mathcal{S}$.

Let $d\mathcal{R}$ denote the infinitesimal rotation and let

$$d\mathcal{S}=d\xi\,d\alpha\,d\theta_{12} \tag{8}$$

denote the infinitesimal variation of shape. Starting from the normalization condition, we have

$$1=\int\mid\Psi_i\mid^2 d\mathbf{r}_1 d\mathbf{r}_2=\int\mid\Psi_i\mid^2\mid J\mid d\mathcal{S}\,d\mathcal{R}\ , \tag{9}$$

where $\mid J\mid$ is the Jacobian arising from the transformation of arguments. From (9) the shape density is naturally defined as

$$\rho_s^i\equiv\mid\Psi_i\mid^2\mid J\mid=\mid\Psi_i\mid^2\xi^5\cos^2\alpha\sin^2\alpha\sin\theta_{12}\ . \tag{10}$$

This quantity is one of the main sources of information on *e-e* correlations that quantum mechanics can provide. Since only $L=0$ states are concerned here, ρ_s^i are orientation independent; thus, in the following, they are only a function of r_1, r_2, and θ_{12}, and are denoted as $\rho_s^i(r_1,r_2,\theta_{12})$.

III. RESULTS AND DISCUSSIONS

The calculated eigenenergies of the $^1S^e$ states with acceptable η_i ($\eta_i\leq 0.03$) are listed in Table I. Some experimental data and some theoretical results from other authors[6–9] are also listed there. The states are first roughly classified as (N,k), where k is simply a serial number of a state in the spectrum converging to the Nth limit of He^+. However, it is well known that there are subseries. Thus, in the following, we shall use the ${}_m(K,T)_N^A$ scheme[10] for a more detailed and more physical classification. K,T,A are quantum numbers labeling the subseries and m is a serial number of a state in a subseries.

In the investigation of the one-body density $\bar{\rho}_1^i$ of all states, we found essentially two types of patterns. In Fig. 1 the $\bar{\rho}_1^i$ of the heads of three series denoted by ${}_1(0,0)_1^+$, ${}_1(1,0)_2^+$, and ${}_1(2,0)_3^+$, respectively, are plotted. There is one dominant peak in each state; outside this peak there is no structure, and inside this peak there may be small inner peaks. The inner peaks (if there are any) are very small. The probability of both electrons staying inside the dominant peak is the largest such that they have similar distances from the center. Another type of pattern is shown in Fig. 2 where the $\bar{\rho}_1^i$ of the $k=8$ and 9 states of the $N=2$ series [denoted by ${}_4(-1,0)_2^+$ and ${}_5(1,0)_2^+$, respectively] have been plotted. There are many outer peaks outside the dominant peak. These outer peaks are very similar to those of the excited states of the hydrogen atom (besides a shift in phase). All $\bar{\rho}_1^i$ of other calculated states differ from those shown in Figs. 1 or 2 only in the locations and number of peaks but not in the essential features.

In the following, we first discuss the first type of state. The locations of the dominant peaks of the $\bar{\rho}_1^i$ of the ${}_1(0,0)_1^+$, ${}_1(1,0)_2^+$, and ${}_1(2,0)_3^+$ states are specified by r_p and are given in Table II. The mean radius and the root-mean-square radius of each state are also given there. From this table we know that the sizes of the ${}_1(1,0)_2^+$ and ${}_1(2,0)_3^+$ states are much larger than that of the ground state. These results are compared with those of the associated states of He^+ and a remarkable increase in size is found due to *e-e* repulsion.

The most probable shapes of these states are given via the optimal values of θ_{12}, r_1, and r_2 (denoted by $\bar{\theta}_{12}$, $\bar{r}_1$, and $\bar{r}_2$) where the shape densities arrive at their maxima; they are given in Table III. From this table we know that the most probable shapes of the heads of each series are isosceles, and they get more and more flat when energy increases.

It should be noted that the structure of this system is determined by a competition between the attractive Coulomb potential and the repulsive *e-e* interaction. If the former is dominant, higher partial waves will be greatly suppressed. On the other hand, if the *e-e* interaction is dominant, the electrons will be kept on opposite sides. For this purpose, there must be a strong angular correlation between the electrons, and the introduction of higher partial waves is inevitable. Thus, in order to understand the competition, one must first make a partial-

TABLE I. Calculated eigenenergies of the three lowest series of the $^1S^e$ states together with the experimental data and with results from other authors.

States	Energies (eV) This paper	Expt. data	States	Energies (eV) This paper	Other authors		
(1,1)	−78.968	−79.014	(2,1)	−21.178	−21.054[a]	−21.167[b]	−21.010[d]
(1,2)	−58.385	−58.400	(2,2)	−16.850	−16.006[a]	−16.924[b]	−16.471[d]
(1,3)	−56.082	−56.095	(2,3)	−16.068	−15.915[a]	−16.053[b]	−15.901[d]
(1,4)	−55.329	−55.341	(2,4)	−14.903	−14.723[a]	−14.914[b]	−14.799[d]
(1,5)	−54.992	−55.003	(2,5)	−14.817			
(1,6)	−54.811	−54.823	(2,6)	−14.354			
(1,7)	−54.704	−54.716	(2,7)	−14.325			
			(2,8)	−14.093			
			(2,9)	−14.080			
$He^+(N=1)$	−54.423		(2,10)	−13.948			
			(2,11)	−13.940			
			(2,12)	−13.858			
			(2,13)	−13.854			
			$He^+(N=2)$	−13.606			
			(3,1)	−9.718	−9.620[c]	−9.603[d]	
			(3,2)	−8.515	−8.638[c]	−8.359[d]	
			(3,3)	−7.685	−7.650[c]	−7.586[d]	
			(3,4)	−7.153	−7.170[c]	−7.007[d]	
			(3,5)	−7.025	−7.004[c]	−6.943[d]	
			(3,6)	−6.865			
			(3,7)	−6.714			
			(3,8)	−6.653			
			(3,9)	−6.568			
			(3,10)	−6.505			
			(3,11)	−6.467			
			(3,12)	−6.415			
			(3,13)	−6.360			
			(3,14)	−6.337			
			(3,15)	−6.318			
			(3,16)	−6.283			
			(3,17)	−6.263			
			(3,18)	−6.250			
			$He^+(N=3)$	−6.047			

[a]Reference 6.
[b]Reference 7.
[c]Reference 8.
[d]Reference 9.

wave analysis.

Let Ψ_i be rewritten as

$$\Psi_i = \sum_l \psi_i^l \ , \tag{11}$$

where l is the angular momentum of an electron and ψ_i^l is the l-wave component of Ψ_i. Let

$$B_i^l = \int | \psi_i^l |^2 d\mathbf{r}_1 d\mathbf{r}_2 \ , \tag{12}$$

which is the weight of the l-wave component. These quantities are shown in Table IV. From this table we know that the attractive potential suppresses the higher partial waves very successfully. This is a victory of the potential. In the lowest series all states are dominated by the S wave. When both electrons are in the S wave, the distribution will be isotropic, and accordingly, the most probable shape will have $\bar{\theta}_{12}=90°$ (due to a larger volume element in phase space). However, there is a well-known property of bound Coulomb wave functions, namely, the degeneracy of different l states having the same n ($n > l$). This basic character plays a very important role in determining the atomic structure. It implies that once the electrons get excited, the intrusion of higher partial waves is inevitable, resulting in a stronger angular correlation and, accordingly, a stronger effect of e-e repulsion. Tables III and IV tell us quantitatively how the intrusion of higher partial waves results in flattening the isosceles. Undoubtedly, the most probable shape of the head of each series will tend to a straight line (a true dumbbell shape) when N increases.

In order to see how ρ_s^i is distributed around its max-

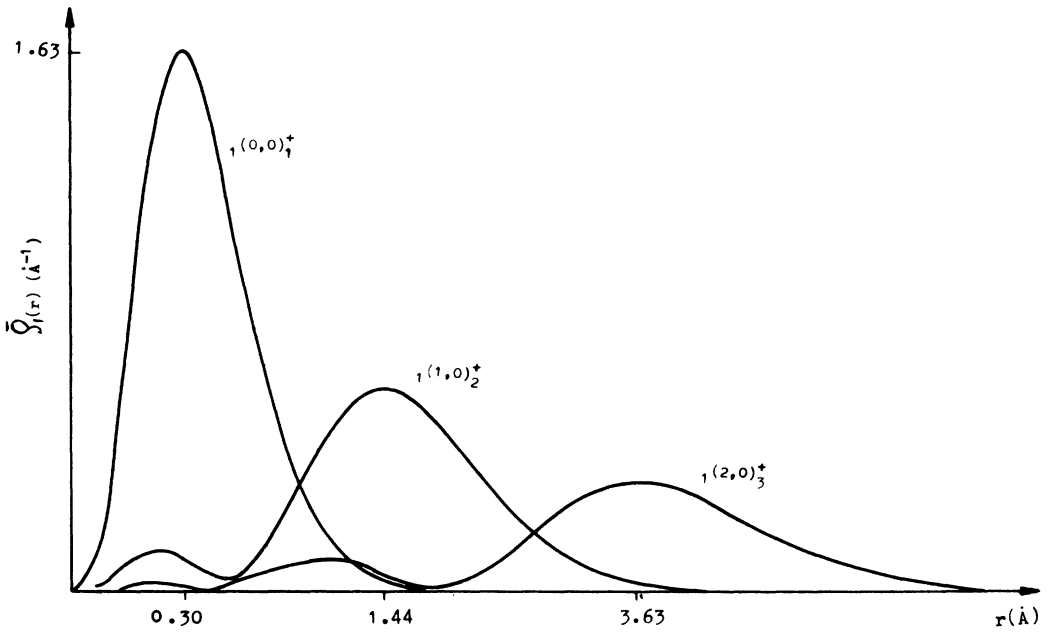

FIG. 1. One-body densities $\bar{\rho}_1(r)$ of the heads of the three lowest $^1S^e$ series: $_1(0,0)_1^+$, $_1(1,0)_2^+$, and $_1(2,0)_3^+$. The abscissa is proportional to $r^{2/3}$. In all the following figures, the coordinates associated with the distance r are proportional to $r^{2/3}$.

imum, we plotted, in Figs. 3(a)–3(c), ρ_s^i as a function of r_1 and r_2 when θ_{12} is given at its optimized value $\bar{\theta}_{12}$. Besides the difference in the degree of excitation, there is a common feature in these figures: a strong background of two symmetrized oscillations with equal amplitude can be seen. They are consistent with those given by Lin[10(d)] (the volume charge density plotted there differs from the shape density here only by a factor of $\sin\theta_{12}$) and those given by Fano.[11]

Figure 3 cannot provide us with a complete picture of *e-e* correlation because the angular correlation has been ignored. To remedy this, we fix r_1 at a series of values. In each case we plot the contour of ρ_s^i as a function of r_2 and θ_{12} and inspect how these contours change in accord with the change of r_1. In this way, we can understand how the motions of two electrons are correlated with each other.

In Fig. 4 the ρ_s^i of $_1(0,0)_1^+$ state is shown in a polar plot of r_2 and θ_{12} when r_1 is given at its optimized value $\bar{r}_1$ (0.40 Å). The shape associated with the peak in this figure is the most probable shape of this state. The distribution of ρ_s^i is broad and thus the geometric shape of this state is not well defined. In order to see the response of the second electron to the motion of the first one, we

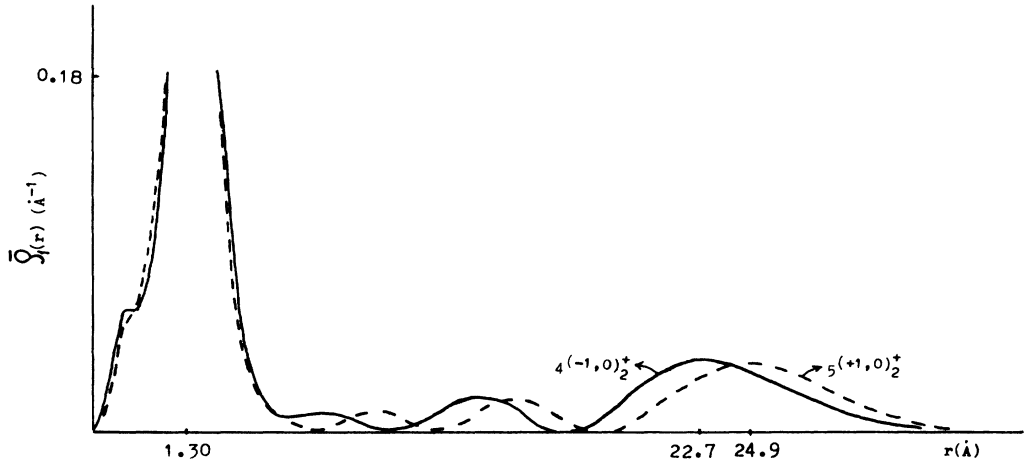

FIG. 2. $\bar{\rho}_1(r)$ of the $_4(-1,0)_2^+$ and $_5(+1,0)_2^+$ states. The coordinates associated with the distance r are proportional to $r^{2/3}$.

TABLE II. r_p (location of the dominant peak of $\bar{\rho}_1$), $\bar{r}$ (mean radius), and $(\bar{r}^2)^{1/2}$ (root-mean-square radius) of the $_1(0,0)_1^+$, $_1(1,0)_2^+$, and $_1(2,0)_3^+$ states. These data are compared with those of the associated states of the helium ion He^+.

	r_p (Å)	$\bar{r}$ (Å)	$(\bar{r}^2)^{1/2}$ (Å)
$_1(0,0)_1^+$	0.30	0.493	0.579
$He^+(1S)$	0.26	0.397	0.458
$_1(1,0)_2^+$	1.44	1.73	1.95
$He^+(2S)$	1.39	1.59	1.72
$_1(2,0)_3^+$	3.63	3.84	4.12
$He^+(3S)$	3.47	3.57	3.80

change r_1 and then observe the corresponding change of the conditional maximum of the shape density labeled as

$$\rho_s^{i,\max}(r_1,\bar{r}_2(r_1),\bar{\theta}_{12}(r_1)) .$$

In this expression $\bar{r}_2$ and $\bar{\theta}_{12}$ are functions of r_1 and they together give the trajectory of the conditional maximum in accord with the change of r_1. When e_1 (the first electron) comes in from 1 to 0.04 Å, the response of e_2 is represented by a motion from point A to point B along the trajectory marked in the figure. The trajectory shows that when e_1 comes in, e_2 tends to go out (together with a small change in $\bar{\theta}_{12}$). This fact reveals the existence of radial-radial (RR) correlation, while the radial-angular (RA) correlation is weak. The RR correlation is in reverse phase and it takes place mainly in a restrained region of r_1 (and r_2) from 0.6 to 0.2 Å.

In Fig. 5(a), the ρ_s^i of the $_1(1,0)_2^+$ state is plotted as a function of r_2 and θ_{12} when r_1 is given at 1.61 Å. The contours show that the distribution of ρ_s^i is relatively sharper and there is an explicit preference for the angle θ_{12}. When e_1 moves from 2.5 to 0.65 Å, the associated change of e_2 is from point A to point B, marked in Fig. 5(a). This is mainly a RR correlation in reverse phase. However, when e_1 moves from 0.65 to 0.45 Å, a very strong radial-angular correlation takes place; the optimal value of θ_{12} [denoted by $\bar{\theta}_{12}(r_1)$] changes dramatically from 135° to 43°. This fact is shown in Figs. 5(b) and 5(c). When r_1 reduces further, $\bar{\theta}_{12}$ moves back monotonically until it equals 90°. We call the region of r_1 where strong RA correlation takes place a SRACR; e.g., there is none in $_1(0,0)_1^+$ but one in $_1(1,0)_2^+$ (r_1 from 0.65 Å to zero).

At the head of the $N=3$ series we found that there are two SRACR's. One appears at r_1 from 0.65 Å to zero

TABLE III. The most probable shapes of the $_1(0,0)_1^+$, $_1(1,0)_2^+$, and $_1(2,0)_3^+$ states. $\bar{r}_1$, $\bar{r}_2$, and $\bar{\theta}_{12}$ are values of r_1, r_2, and θ_{12} where ρ_s arrives at its maximum.

	$\bar{\theta}_{12}$	$\bar{r}_1(=\bar{r}_2)$ (Å)
$_1(0,0)_1^+$	100°	0.40
$_1(1,0)_2^+$	135°	1.61
$_1(2,0)_3^+$	142°	3.85

TABLE IV. Weight B_i^l of different partial-wave components of the $_1(0,0)_1^+$, $_1(1,0)_2^+$, and $_1(2,0)_3^+$ states.

	B_i^S	B_i^P	B_i^D	B_i^F
$_1(0,0)_1^+$	0.996	0.004	0	0
$_1(1,0)_2^+$	0.726	0.273	0.001	0
$_1(2,0)_3^+$	0.550	0.409	0.040	0

where $\bar{\theta}_{12}$ falls suddenly from 142° to 43° and then increases monotonically to 90° as before. The second one appears around $r_1=1.90$ Å; when r_1 decreases in this narrow region, $\bar{\theta}_{12}$ falls suddenly from 142° to 43° and then increases rapidly back to 142°.

Now let us discuss the results of the second type of state as represented by Fig. 2. Nearly all states besides the heads of the series belong to this type, where one electron is much farther away than the other one.

We find that all $_m(0,0)_1^+$ states are dominated by the S-wave component. The dominant peaks of $\bar{\rho}_1^i$ are all located at about 0.27 Å (an exception is the $_1(0,0)_1^+$ state were 0.30 Å is found). Thus the dominant peaks are very close to that of the ground state of He^+. On the other hand, we find that the outer peaks of $\bar{\rho}_1^i$ are very close to those of the hydrogen atom with a very small shift in phase. Thus we can conclude that in the first series the e-e correlation is very weak. The dynamical background of the suppression of e-e correlation is evident from the above discussion, i.e., the higher partial waves are suppressed by the Coulomb potential such that the electrons are not able to have strong angular correlation with each other.

All the $N=2$ states are dominated by a strong mixture of S and P waves, and other partial waves are inconsiderable. All the dominant peaks of $\bar{\rho}_1^i$ are located from 1.26 to 1.34 Å [except that in the $_1(1,0)_2^+$ state, which is larger]. Contrary to the $N=1$ series, the outer peaks are shifted from those of the hydrogen atom explicitly. From the investigation of the shape density, we found that all the $k=$odd states have $\bar{\theta}_{12}=135°$ and thus can be denoted as $_m(1,0)_2^+$ with $k=2m-1$; all the $k=$even states have $\bar{\theta}_{12}=45°$ and thus can be denoted as $_m(-1,0)_2^+$ with $k=2m$. We further found the following:

(i) Accidentally, when $m\geq 3$, the energy of the $_m(-1,0)_2^+$ state is extremely close to its adjacent higher state, the $_{m+1}(1,0)_2^+$ state; they are nearly degenerate. For example, the energy difference of $_4(-1,0)_2^+$ and $_5(1,0)_2^+$ is 0.013 eV, while that of $_5(1,0)_2^+$ and $_5(-1,0)_2^+$ is 0.132 eV. Besides, they are similar in size: the mth $K=-1$ state is only a little smaller than the $(m+1)$th $K=+1$ state (the size is measured by the location of the outmost peak r_{out} of $\bar{\rho}_1^i$). For example, the r_{out} of $_4(-1,0)_2^+$ and $_5(1,0)_2^+$ are 22.7 and 24.9 Å, respectively, while that of the $_5(-1,0)_2^+$ state is 33.6 Å.

(ii) In the $K=1$ ($k=$odd) subseries, the S wave is dominant at the beginning; e.g., in the $_1(1,0)_2^+$ state we have $B_i^S=0.73$. However, as m increases, the P wave gradually gets stronger; when $m\geq 4$, $B_i^P=0.55$ and $B_i^S=0.45$.

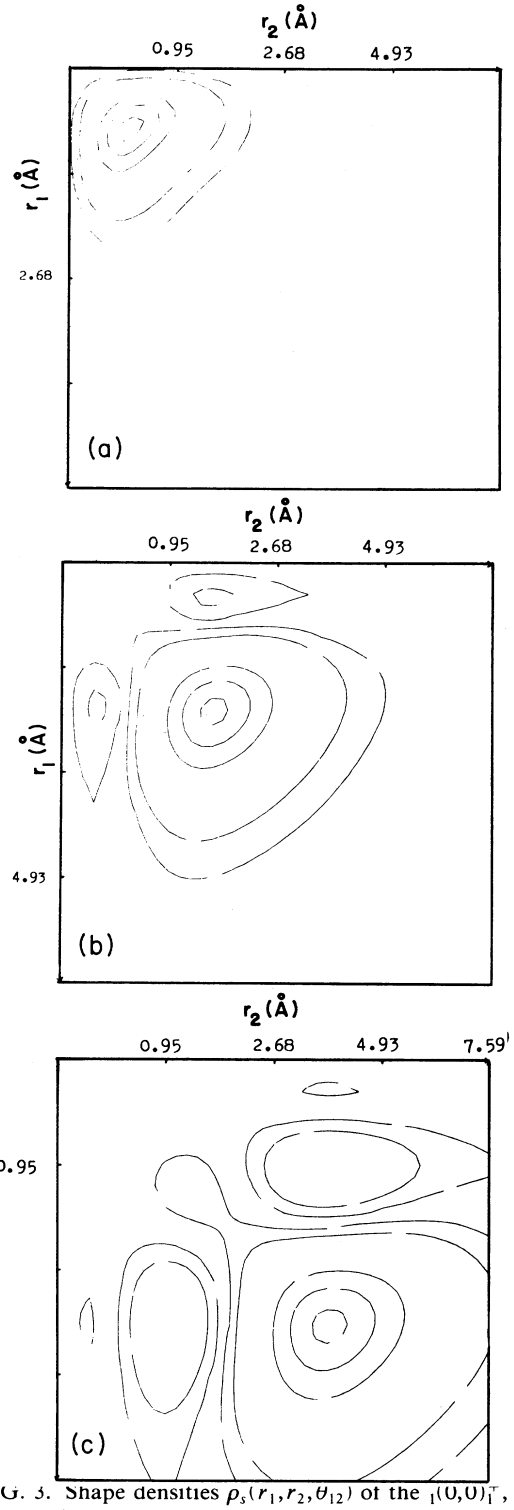

FIG. 3. Shape densities $\rho_s(r_1,r_2,\theta_{12})$ of the $_1(0,0)_1^+$, $_1(1,0)_2^+$, and $_1(2,0)_3^+$ states plotted in (a), (b), and (c), respectively, as a function of r_1 and r_2 when θ_{12} is fixed at its optimal values $\bar{\theta}_{12}$, i.e., $\bar{\theta}_{12}=100°$, 135°, and 142°, respectively. The contours from inward to outward having $\rho_s=\alpha\rho_s^{\max}$ with $\alpha=\frac{19}{20}$, $\frac{15}{20}$, $\frac{10}{20}$, $\frac{1}{20}$, and $\frac{1}{100}$. Here $\rho_s^{\max}$ is the largest value of ρ_s in the figure (the values of α are the same in the following figures; however, in many cases the contour having $\alpha=\frac{1}{100}$ does not appear). (a)–(c) show the distribution of ρ_s around their most probable shapes. Note that the ordinate and the abscissa are proportional to $r_1^{2/3}$ and $r_2^{2/3}$, respectively.

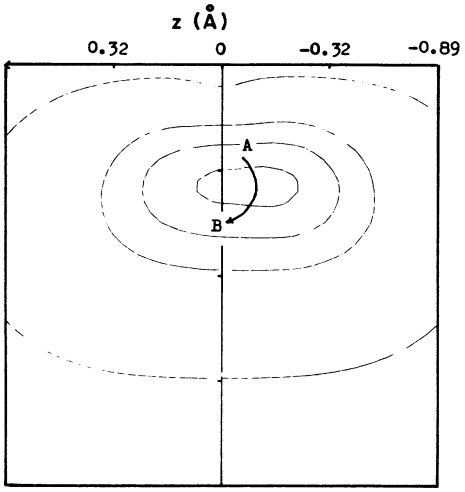

FIG. 4. ρ_s of the $_1(0,0)_1^+$ state as a function of the location of e_2 when e_1 is given at 0.40 Å along the $+z$ axis. A vector originating from the origin gives the direction of $\mathbf{r}_2$, while its norm is proportional to $r_2^{2/3}$. Values of α are the same as those in Fig. 3.

In the $K=-1$ (k=even) subseries, the P wave is dominant at the beginning; e.g., in the $_1(-1,0)_2^+$ state we have $B_i^P=0.65$. However, as m increases, the S wave gradually gets stronger; when $m\geq 4$, $B_i^S=0.55$ and $B_i^P=0.45$.

An example of the difference in $\bar{\rho}_1^i$ between the $K=+1$ and -1 subseries is shown in Fig. 2. A small inner peak of the $K=-1$ state can be seen arising from S-wave oscillation, while that of the $K=+1$ state is not explicit. The number of outer peaks increases with m, revealing the degree of excitation.

The shape density of the $_3(-1,0)_2^+$ and $_4(1,0)_2^+$ states are plotted in Figs. 6(a) and 6(b) as a function of r_1 and r_2 when θ_{12} is given at its optimized value $\bar{\theta}_{12}$. A comparison of these figures with Figs. 3(a)–3(c) reveals the great difference between the two types of states. Though Fig. 6(a) is similar to 6(b), they are different in the inner region (both r_1 and r_2 are small). This difference is a noticeable point in distinguishing the structure of the $K=+1$ and -1 states, because the inner region is an important region where very strong energy and momentum transfer may occur between the electrons. Besides, the locations of the maxima in the outer region are not one-to-one identical.

As before, we observe the variation of the conditional maxima of ρ_s^i when the prescribed location of an electron changes. We find again the existence of the SRACR's in all the states of this series. In a $_m(\pm 1,0)_2^+$ state there are $(m-1)$ SRACR's. Some examples are listed in Table V, where we find the following.

(i) For the $K=+1$ states, when r_1 decreases inside a SRACR, $\bar{\theta}_{12}$ changes from 135°→45°→135° (in the innermost SRACR, it is 135°→45°→90°). The locations of the SRACR's of the mth state nearly overlap with those of the $(m+1)$th state [except the outmost one of the $(m+1)$th state, which has no counterpart]. Since the SRACR is only a very narrow region, we can say that the

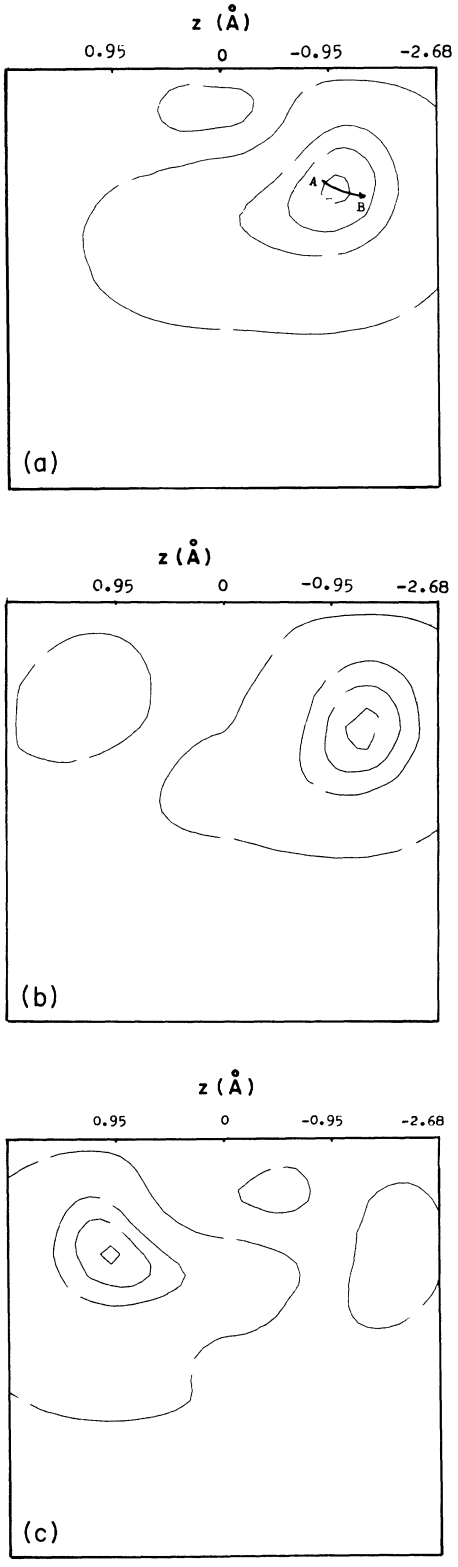

FIG. 5. ρ_s of the $_1(1,0)_2^+$ state as a function of the location of e_2 when e_1 is given at 1.61, 0.65, and 0.45 Å, respectively, along the $+z$ axis. In (a) the distribution of ρ_s around its maximum is shown. In (b) and (c), a great change in $\bar{\theta}_{12}(r_1)$ in accord with only a small change in r_1 in the SRACR is shown. The coordinates associated with the distance r are proportional to $r^{2/3}$. Values of α are the same as those in Fig. 3.

$K=+1$ states mostly have $\bar{\theta}_{12}=135°$.

(ii) For the $K=-1$ states, the above discussion holds, except that 135° should be interchanged with 45°.

The appearance of the SRACR surely implies that the way of interference of (at least) two partial waves changes back and forth in this narrow region. The exact location of a SRACR is determined by a pair of nodes. We will study the SRACR from a detailed analysis of the interference of partial waves and the results will be reported elsewhere. The detailed results of the $N=3$ series will also be reported elsewhere.

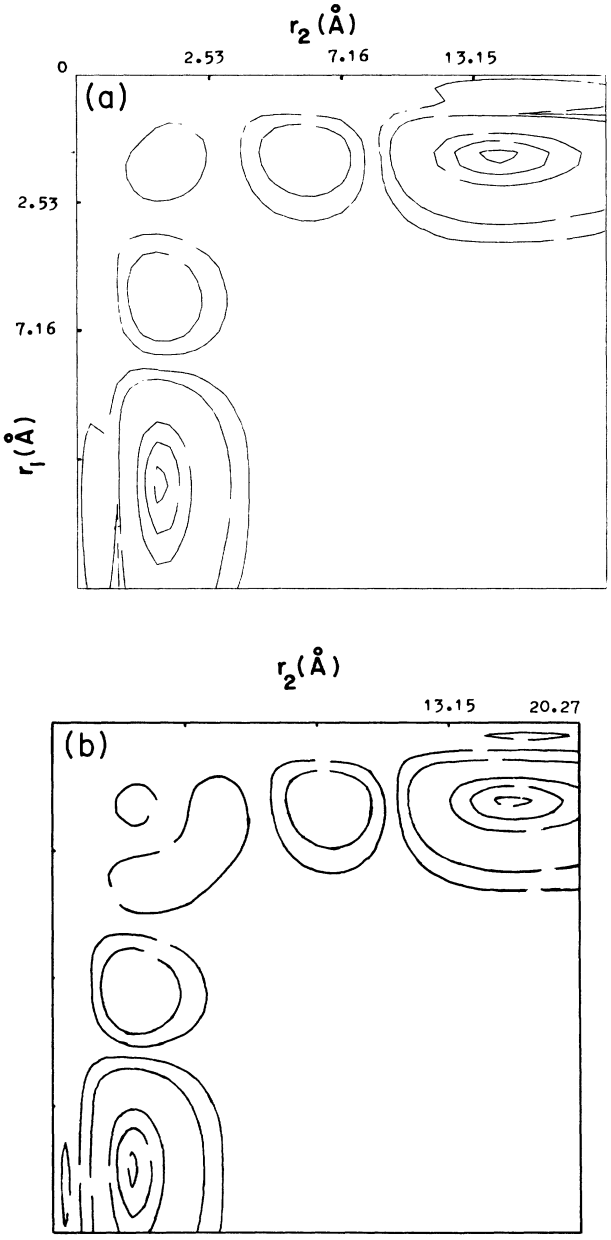

FIG. 6. ρ_s of the $_3(-1,0)_2^+$ and $_4(+1,0)_2^+$ states as a function of r_1 and r_2 when θ_{12} is given at $\bar{\theta}_{12}=45°$ and 135°, respectively. The coordinates associated with the distance r are proportional to $r^{2/3}$. Values of α are the same as those in Fig. 3.

IV. SUMMARY

We worked in a space that is a union of four spaces, each spanned by a finite set of basis functions. After the diagonalization of the Hamiltonian, we obtained the eigenfunctions which have been analyzed in detail. The accuracy of these solutions has also been evaluated. We emphasize that the aim of this work was not to develop an accurate method to fit the experimental spectrum better; instead, its aim was to obtain qualitative features of the *e-e* correlation from a systematic analysis of the wave functions to understand better the structure and internal motion of the helium atom. In fact, most of our effort has been devoted to this analysis.

The dynamical background underlying the structures of atoms is the competition between the attractive Coulomb potential and the *e-e* interaction. The realization of the *e-e* correlation relies seriously on the interference of different partial waves. However, the Coulomb potential imposes stern restrictions on the angular motion of the electrons and thus suppresses higher partial waves and, accordingly, the effect of *e-e* interaction. Only when both electrons are sufficiently energetic to include high partial waves, can the *e-e* interaction play its role sufficiently in atomic structures.

We found that in the $_1(0,0)_1^+$ state (the ground state), the *e-e* correlation is weak, which is essentially an RR correlation in reverse phase. In the higher $_m(0,0)_1^+$ states the *e-e* correlation is even weaker.

The mixing of S and P waves in the second series and the mixing of S, P, and D waves in the third series is remarkable, which implies the existence of a much stronger *e-e* correlation, and, accordingly the shape of the system can be now better defined. A pioneer work in Ref. 12 stated the existence of the dumbbell shape. In this paper, the most probable shapes of the states have been investigated in a systematic manner. A pioneer work in group-theory analysis stated the K-classification scheme of the spectrum,[13] which has been justified by microscopic adiabatic calculation.[10] In this paper, from a nonadiabatic calculation and from an analysis of the shape density, we recover again the K-classification scheme, and show that the origin of this classification is the interference of partial waves. In fact, in our analysis of the wave functions, we emphasize the decomposition of Ψ_i into different partial-wave components. This decomposition turns out to be a useful way to reveal the similarity and the difference in internal structure among the excited states.

Special effort has been made to investigate the response of an electron to the motion of the other one. This is a way to understand the internal motion better. In the second type of state, one electron is much farther away than the other one. At first glance, one would suggest that the *e-e* correlation was weak and the outer electron simply moved freely in a Coulomb potential screened by the inner electron. However, this suggestion fails. The discovery of the SRACR is striking, and implies that the outer electron has a remarkably strong RA correlation with the inner one in some narrow regions. It is important to remember that in the case of total angular momentum L being zero, if an electron rotates, the other one must rotate accordingly in the reverse direction, to

TABLE V. Variation of $\tilde{\theta}_{12}(r_1)$ of the $K=\pm1$ states of the $N=2$ series in accord with r_1, with the existence of the SRACR's and their locations.

			SRACR		SRACR		SRACR
$K=-1$ states	$_3(-1,0)_2^+$	r_1		$+\infty\rightarrow10$ Å	10 Å→8.5 Å→7 Å	7 Å→0.65 Å	0.65 Å→0.45 Å→0
		$\tilde{\theta}_{12}(r_1)$		~45°	45°→135°→45°	~45°	45°→135°→90°
	$_4(-1,0)_2^+$	r_1	$+\infty\rightarrow17$ Å	17 Å→15.4 Å→13 Å	13 Å→9 Å	9 Å→8 Å→6.5 Å	6.5 Å→0.65 Å	0.65 Å→0.45 Å→0
		$\tilde{\theta}_{12}(r_1)$	~45°	45°→135°→45°	~45°	45°→135°→45°	~45°	45°→135°→90°
$K=+1$ states	$_3(+1,0)_2^+$	r_1			$+\infty\rightarrow6.5$ Å	6.5 Å→5.5 Å→4.5 Å	4.5 Å→0.75 Å	0.75 Å→0.45 Å→0
		$\tilde{\theta}_{12}(r_1)$			~135°	135°→45°→135°	~135°	135°→45°→90°
	$_4(+1,0)_2^+$	r_1	$+\infty\rightarrow11.8$ Å	11.8 Å→10.3 Å→9.5 Å	9.5 Å→6 Å	6 Å→5.3 Å→3.8 Å	3.8 Å→0.75 Å	0.75 Å→0.45 Å→0
		$\tilde{\theta}_{12}(r_1)$	135°	135°→45°→135°	~135°	135°→45°→135°	~135°	135°→45°→90°

conserve L. Since, inside the SRACR, $\tilde{\theta}_{12}$ changes dramatically, we conclude that the electron passes through the SRACR in a wiggly manner. The origin of this wiggly motion is the dramatical change in partial-wave composition in these narrow regions. This motion is a feature of two- (or more) electron systems, and does not appear in hydrogenlike atoms.

Though we have found some interesting qualitative features, the quantitative results have to be refined and more states (e.g., those states with L not equal to zero or with antisymmetric permutation symmetry) have to be included in this kind of analysis to obtain more systematic information, to understand better the helium atom.

ACKNOWLEDGMENTS

The author is obliged to Professor E. W. Schmid and Professor W. Glöckle for their warm hospitality during his stay in Germany. He highly appreciates the discussion with them and with Dr. Walliser and Dr. Spitz in Tübingen, which was very helpful and necessary to this work. The author is also obliged to the Alexander von Humboldt Foundation for its support. This work was supported by the Science Fund of the Chinese Academy of Sciences.

[1]U. Fano, Rep. Prog. Phys. **46**, 97 (1983).

[2]A. R. P. Rau, in *Atomic Physics,* edited by R. S. Van Dyck and E. N. Fortson (World Scientific, Singapore, 1984), Vol. 9.

[3]C. D. Lin, in *Few-Body Methods: Principles & Applications,* edited by T. K. Lim, C. G. Bao, D. P. Hou, and H. S. Huber (World Scientific, Singapore, 1986), p. 507; M. I. Haftel, *ibid.*, p. 793.

[4]C. G. Bao, in *Few-Body Methods: Principles & Applications,* edited by T. K. Lim, C. G. Bao, D. P. Hou, and H. S. Huber (World Scientific, Singapore, 1986), p. 581; C. G. Bao, G. C. Qiu, H. D. Cao, Y. P. Gan, L. X. Luo, and T. K. Lim, Few-Body Syst. **2**, 81 (1987).

[5]E. A. Hylleraas, Z. Phys. **48**, 429 (1928); H. Shull and P. O. Löwdin, J. Chem. Phys. **23**, 1362 (1955); **30**, 617 (1959).

[6]J. Macek, J. Phys. B **1**, 831 (1968).

[7]Y. K. Ho, Phys. Rev. A **23**, 2137 (1980).

[8]Y. K. Ho, J. Phys. B **12**, 387 (1979).

[9]N. Koyama, H. Fukuda, T. Motoyama, and M. Matsuzawa, J. Phys. B **19**, L331 (1986).

[10](a) C. D. Lin, Phys. Rev. A **12**, 493 (1975); (b) **14**, 30 (1976); (c) **23**, 1585 (1981); (d) **25**, 76 (1982); (e) **25**, 1535 (1982); (f) **29**, 1019 (1984).

[11]U. Fano, in *The Physics of Electronic and Atomic Collisions,* Invited Lectures, Review Papers, and Progress Reports of the Ninth International Conference on the Physics of Electronic and Atomic Collisions, Seattle, 1975, edited by J. S. Risley and R. Gaballe (University of Washington Press, Seattle, 1976), p. 27.

[12]R. Berry, G. S. Ezra, and G. Natanson, in *New Horizons of Quantum Chemistry,* edited by P. O. Löwdin and B. Pullman (Reidel, Dordrecht, Holland, 1983), p. 77.

[13]D. R. Herrick and O. Sinanoglu, Phys. Rev. A **11**, 97 (1975).